9. Lewis, J. S. Satellites of the outer planets: thermal models. *Science* **172,** 1127–1128 (1971).
10. Consolmagno, G. J. & Lewis, J. S. The evolution of icy satellite interiors and surfaces. *Icarus* **34,** 280–293 (1978).
11. Stevenson, D. J. An ocean within Callisto? *Eos* **79,** F535 (1998).
12. Kargel, J. S. Ammonia-water volcanism on icy satellites: Phase relations at 1 atmosphere. *Icarus* **100,** 556–574 (1992).
13. Kargel, J. S. *et al*. Europa's crust and ocean: origin, composition, and the prospects for life. *Icarus* **148,** 226–265 (2000).
14. Sotin, C., Grasset, O. & Beauchesne, S. in *Solar System Ices* (eds Schmitt, B., De Bergh, C. & Festou, M.) 79–96 (Kluwer Academic, Dordrecht, 1998).
15. Goldsby, D. L. & Kohlstedt, D. L. Grain boundary sliding in fine-grained ice I. *Scripta Mater.* **37,** 1399–1406 (1997).
16. Pappalardo, R. T. *et al*. Geological evidence for solid-state convection in Europa's ice shell. *Nature* **391,** 365–368 (1998).
17. McKinnon, W. B. Convective instability in Europa's floating ice shell. *Geophys. Res. Lett.* **26,** 951–954 (1999).
18. Goldsby, D. L. & Kohlstedt, D. L. Superplastic deformation of ice: Experimental observations. *J. Geophys. Res.* (in the press).
19. Durham, W. B., Kirby, S. H. & Stern, L. A. The rheology of ice I at low stress and elevated confining pressure. *J. Geophys. Res.* (in the press).
20. Goldsby, D. L. & Kohlstedt, D. L. Flow of ice I by dislocation, grain boundary sliding, and diffusion processes. *Lunar Planet. Sci.* **XXVIII,** 429–430 (1997).
21. Showman, A. P. & Malhotra, R. Tidal evolution into Laplace resonance and the resurfacing of Ganymede. *Icarus* **127,** 93–111 (1997).
22. Klinger, J. Influence of a phase transition of the ice on the heat and mass balance of comets. *Science* **209,** 271–272 (1980).
23. Mueller, S. & McKinnon, W. B. Three-layered models of Ganymede and Callisto: Compositions, structures, and aspects of evolution. *Icarus* **76,** 437–464 (1988).
24. Kirk, R. L. & Stevenson, D. J. Thermal evolution of a differentiated Ganymede and implications for surface features. *Icarus* **69,** 91–134 (1987).
25. Davies, M. E. *et al*. The control networks of the Galilean satellites and implications for global shape. *Icarus* **135,** 372–376 (1998).
26. McKinnon, W. B. in *Solar System Ices* (eds Schmitt, B., De Bergh, C. & Festou, M.) 525–550 (Kluwer Academic, Dordrecht, 1998).
27. Solomatov, V. S. & Moresi, L.-N. Stagnant lid convection on Venus. *J. Geophys. Res.* **101,** 4737–4753 (1996).
28. Lupo, M. J. & Lewis, J. S. Mass-radius relationships in icy satellites. *Icarus* **40,** 157–170 (1978).
29. Durham, W. B., Kirby, S. H. & Stern, L. A. Creep of water ices at planetary conditions: A compilation. *J. Geophys. Res.* **102,** 16293–16302 (1997).
30. Kamb, B. in *Flow and Fracture of Rocks* (eds Heard, H. C., Borg, I. Y., Carter, N. L. & Raleigh, C. B.) 211–241 (AGU Geophys. Monogr. Ser. 16, American Geophysical Union, Washington DC, 1972).

Acknowledgements

I thank F. Anguita, O. Prieto, J. Ruiz, R. Tejero and A. Torices for suggestions, K. Bennett and J. Kargel for comments on the manuscript, and W. Durham and D. Goldsby for preprints of work in press.

Correspondence and requests for materials should be addressed to the author (e-mail: jaruiz@eucmax.sim.ucm.es).

Evidence for recent climate change on Mars from the identification of youthful near-surface ground ice

John F. Mustard, Christopher D. Cooper & Moses K. Rifkin

Department of Geological Sciences, Brown University, Providence, Rhode Island 02912, USA

Ground ice in the crust and soil may be one of the largest reservoirs of water on Mars[1–3]. Near-surface ground ice is predicted to be stable at latitudes higher than 40° (ref. 4), where a number of geomorphologic features indicative of viscous creep and hence ground ice have been observed[5]. Mid-latitude soils have also been implicated as a water-ice reservoir[6], the capacity of which is predicted to vary on a 100,000-year timescale owing to orbitally driven variations in climate[7]. It is uncertain, however, whether near-surface ground ice currently exists at these latitudes, and how it is changing with time. Here we report observational evidence for a mid-latitude reservoir of near-surface water ice occupying the pore space of soils. The thickness of the ice-occupied soil reservoir (1–10 m) and its distribution in the 30° to 60° latitude bands indicate a reservoir of (1.5–6.0) × 10^4 km^3, equivalent to a global layer of water 10–40 cm thick. We infer that the reservoir was created during the last phase of high orbital obliquity less than 100,000 years ago, and is now being diminished.

Using high-resolution images from the Mars Orbiter Camera (MOC) on the Mars Global Surveyor (MGS) spacecraft[8,9], we have identified and mapped on a global scale a unique, young terrain on Mars that exhibits a morphology consistent with a material that has been cemented and then partially dissected (cut into hills and valleys) or disaggregated. The terrain (Fig. 1) is recognized on the basis of the following criteria: (1) a smooth, intact surface is present; (2) the smooth material is broken up or dissected somewhere in the

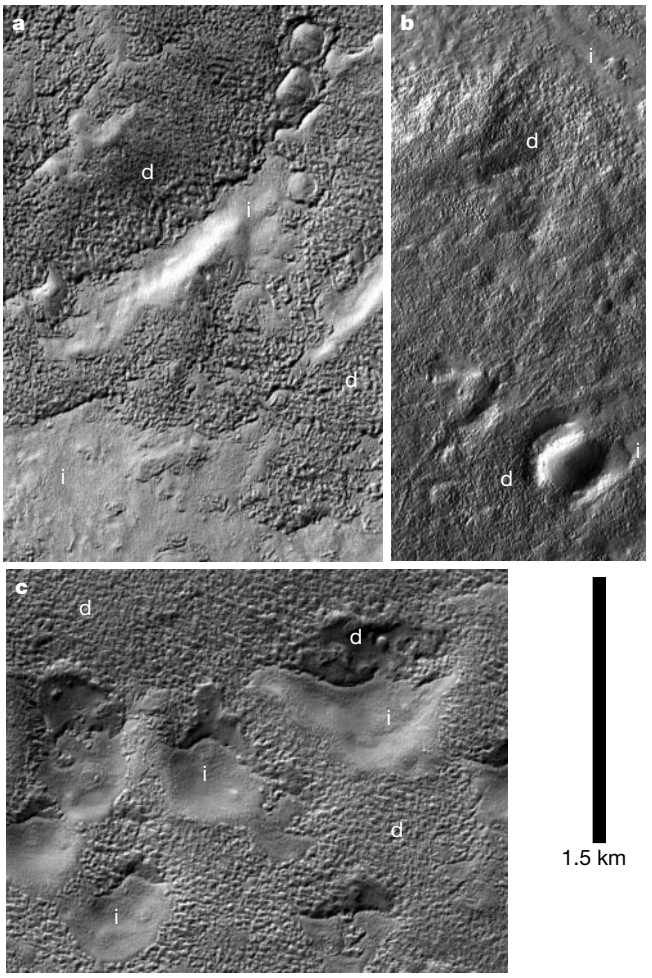

Figure 1 Examples of terrain interpreted to contain near-surface ground ice. The scale is the same for all images and in each image 'i' indicates intact terrain and 'd' indicates dissected (eroded) terrain. Illumination is from below and the nearest pole is towards the top of each image. **a**, A large expanse of intact terrain with incipient dissection into numerous steep-walled pits and troughs a few metres in size. The layer thickness is estimated to be 10 m. **b**, The amount of dissection is greater and clearly demonstrates the lack of preferred orientation and pattern in the dissected terrain. Here the layer thickness is estimated to be 2 m. **c**, The dissected layer in this region, estimated to be 5 m thick, is completely removed in places, revealing the substrate beneath. In these three examples, the density of pits ranges from sparse to abundant. The pitted surface grades into a knobby terrain which further grades into a rough surface. In areas of complete degradation a relict surface is revealed. The gradations between the smooth, pitted, knobby and rough surfaces imply a process where the smooth unit disaggregates and is removed to reveal a pre-existing surface. **a**, Image M0400837 (43.40° N, 240.21° W), $i = 55.31°$; **b**, image SP253404 (34.35° N, 356.00° W), $i = 74.67°$; **c**, image FHA01450 (43.71° S, 239.61° W), $i = 75.49°$.

scene; (3) the pitted or hummocky terrain resulting from dissection is distinct from dunes, yardangs (ridges formed by wind erosion), or other aeolian (wind-driven) features.

We have examined over 8,000 of the narrow-angle MOC images that were acquired prior to August 1999 with a spatial resolution of less than 10 m per pixel. The images were classified by the presence or absence of the terrain as described above and the results are shown in Fig. 2. The eroded terrain is concentrated in two latitude bands: 30° to 70° N and 25° to 65° S. Few occurrences are found between ±30° latitude and at latitudes poleward of ±60°. The total number of images examined and the fraction of images showing dissection, as a function of latitude, are shown in Fig. 3. Two distinct and remarkably similar distributions are observed: they are slightly asymmetric with a steep rise in number from equatorial latitudes but with extended occurrences towards polar latitudes.

Detailed analysis of many of the individual images with this terrain reveals the following general characteristics (Fig. 1). Where this terrain is intact, it forms a mantle of uniform thickness that is superimposed or draped across the topography muting the morphology. This is distinct from mantling in equatorial latitudes where such mantles fill in topographic lows leaving the rough textured surfaces on ridges and high points. The intact unit is very uniform in albedo, appears smooth at the resolution of the MOC images (typically 3 m per pixel), and fresh impact craters of any size are very rare. Pits and remnant ridges exhibit no apparent preferred orientations and the total absence of any layering indicates a lack of internal structure to the mantle layer. By using the shadows adjacent to pits along the azimuth direction of the sun we estimate the thickness of the deposit to range between 1 m and 10 m. Within a given image, estimates of layer thickness are consistent, indicating a discrete thickness to the layer in any given region. There is a conspicuous absence of mobile materials such as dunes associated with this unit; dunes are commonly observed elsewhere on Mars at MOC resolution[9]. Where the layer is completely removed (Fig. 1c), a more stable or solid surface remains apparently unaffected by the process of dissection. The morphology indicates the presence of a mantling material that has sufficient strength to support short, steep slopes.

The material comprising the majority of the mantle is probably dust. There are two models for the existence of a competent surface mantle dominated by dust: a chemical cement or cementation with ground ice. A weakly cemented regolith was observed at the Viking landing sites, in which sulphate salts were considered to be the most likely cement[10]. Surface–atmosphere exchange of adsorbed water provides a mechanism to mobilize highly soluble magnesium sulphate on geological timescales, leading to a cemented mantle. However, an increase in the thermal inertia relative to terrains dominated by loose dust[10], or spectroscopic properties that indicate sulphate-cemented soils[11] associated with the distribution in Fig. 2 are not observed.

The distribution shown in Fig. 2 is strongly associated with the distribution of various viscous creep features, such as lobate debris aprons, lineated valley fill, concentric crater fill, and terrain softening[1,5], that were recognized in Viking images. These viscous creep features have been interpreted to be indicative of ground ice on the basis of thermophysical properties, rheology, and by analogy with features observed in periglacial terrains on Earth[1,5]. In some of the MOC images, the mapped mantle layer exhibits viscous creep and flow features when present on steep slopes[12] as well as patterned ground (for example, polygons)[13]. Although patterned ground is not uniquely indicative of ground ice, viscous creep requires a rheology strongly consistent with an ice-saturated regolith.

Although there are no direct earth analogues for the terrain shown in Fig. 1, the thermophysical and mechanical properties of frozen loess observed in the Fox permafrost tunnel[14] provide an analogue that explains the primary morphologic characteristics. The tunnel temperature is maintained between −2 °C and −5 °C and during the winter dry air flowing through the tunnel causes sublimation of ice from the loess, leaving behind a porous but cohesive material. Over the past 30 years a desiccated layer of the order of 10 cm thick has formed on the walls and ceiling. Although this remnant on the walls and ceiling of the tunnel, it collapses to particulate loess upon slight disturbance. The calculated thermal inertia of desiccated loess under Mars conditions indicates that it would not be distinguishable from loose martian dust. A similar, porous, structured material has been produced in experiments designed to model martian polar materials[15].

In general, the surface winds on Mars predicted from models[16] and measured at the landing sites are too weak to disaggregate a mantle with the strength of bonded loess. However, dust devils, the

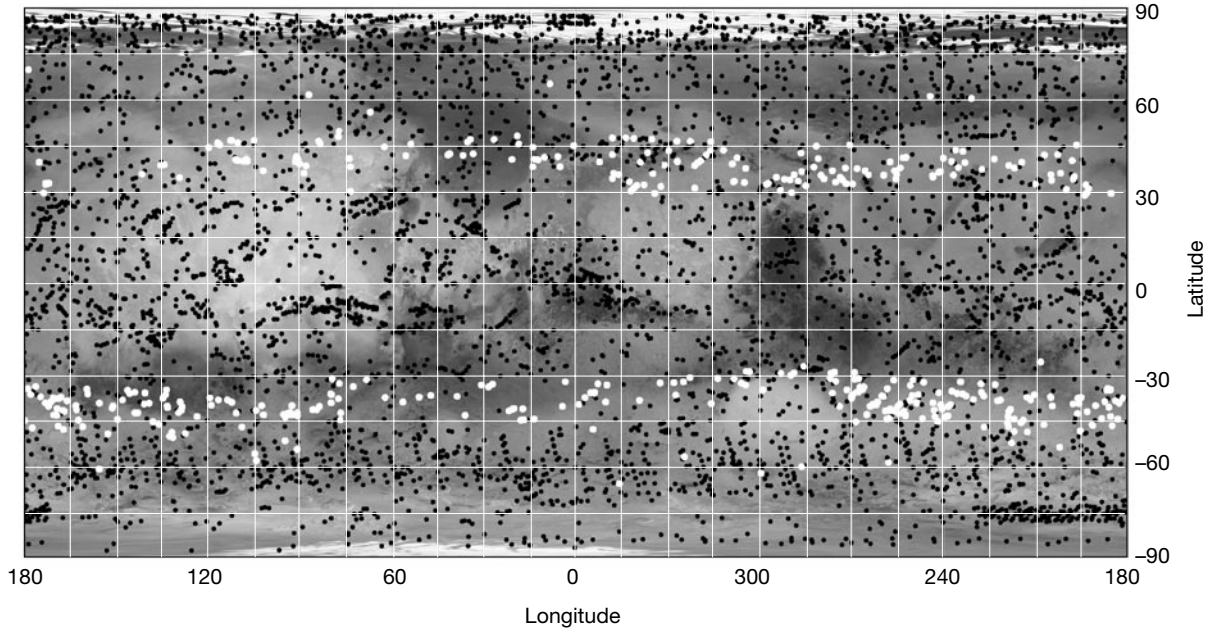

Figure 2 Global distribution of the image locations used in this investigation. Simple cylindrical projection with the global Viking basemap as a background; image locations that exhibit the dissected terrain are shown as white dots and images examined that do not exhibit such terrain are shown in grey dots.

most common energetic surface component of the martian atmosphere yet characterized, do provide the requisite strengths[17,18]. High-pressure gradients between the dust-devil core and ambient conditions (up to 50 Pa difference in pressure) coupled with high wind speeds (typically 25–30 m s^{-1} but may be up to 60 m s^{-1} in the larger events) create surface shear strengths sufficient to disaggregate the dissected mantle. Material liberated by the passage of the dust devil is lofted and dispersed leaving no accumulations of residual material.

On the basis of this evidence, we conclude that this eroded mantle represents regions on Mars where a layer of generally uniform thickness of dust and soil has been permeated and cemented by ice, but that is now in the process of active disaggregation. Airfall deposition concurrent with ice cementation provides a viable mechanism to produce the uniform thickness and lack of internal structure implied by the morphology. The very smooth character of the intact surfaces implies young surfaces. We have not yet observed an unmodified impact crater in the intact surfaces greater than 100 m in diameter; this indicates a surface age of less than 1.5×10^5 years[19]. The bimodal latitude dependence with peaks at

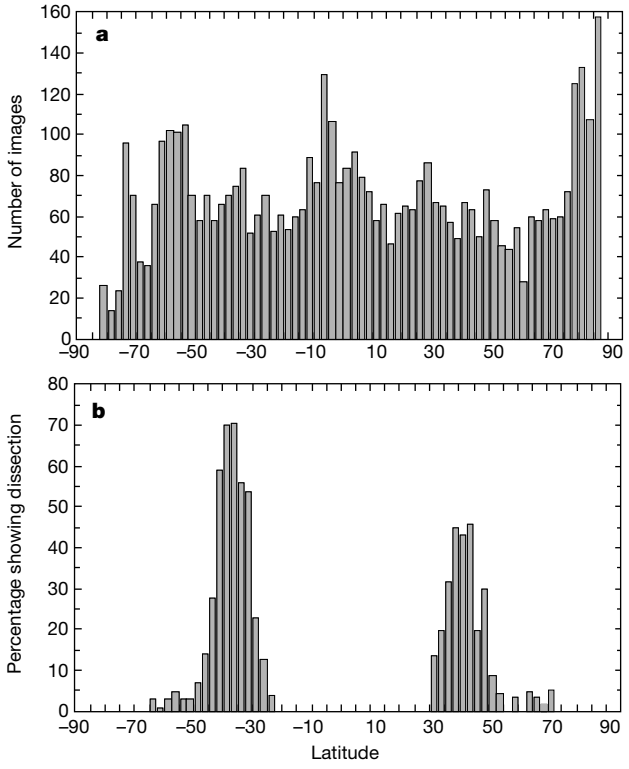

Figure 3 Latitude distribution of MOC frames showing dissection. **a**, Total distribution of images used in this study in 2.5° latitude bins. **b**, Percentage of images shown in **a** that exhibit dissection. For the northern distribution the mean is 41.93°, median is 40.51°, and the standard deviation of the distribution is 10.71°. For the southern distribution the mean is –40.79°, the median –39.95°, and the standard deviation is 10.13°. The equatorward limit of the distributions indicate regions that retain remnant patches of soil-hosted ground ice formed during the last ground-ice maximum. In MOC images that do not exhibit the three components required for identification a uniform mantle is generally absent in the 30° to 40° latitude bands. The poleward limit of the distribution represents regions that are either currently experiencing incipient desiccation and dissection or are remnants of the previous period of minimum ground-ice stability. In MOC images observed for locations poleward of 40° or 50°, a uniform mantle is commonly present. The poleward boundaries of the distributions also correlate with a decrease in topographic roughness calculated with a short 0.6-km baseline using Mars Observer Laser Altimeter (MOLA) data[20]. Because the decrease in short baseline roughness is not accompanied by changes in long baseline roughness, it is interpreted as due to a uniform mantling of the surface poleward of 50°.

±40° (Fig. 3) is the central defining characteristic of the global distribution.

The striking latitude dependence of this terrain provides confirming evidence for a dynamic ground-ice model for Mars[7]. In this spatially explicit diffusion and condensation model, changes in insolation and atmospheric water abundance driven by variations in the eccentricity, obliquity and time of perihelion (precession) result in the formation and removal of ground ice in the top 2–4 m of soil over timescales of 100,000 years, particularly for latitudes greater than 30°. This model predicts that the most recent maximum extent of soil-hosted ground ice was around 100,000 years ago and reached to within 30° of the equator, but the ice has since retreated. Ground ice is currently predicted to be stable in the martian soil poleward of 40° (refs 4, 7) although the exact latitude depends on the local thermophysical properties. The equatorward limit of the distribution shown in Fig. 3 thus indicates regions of the surface that retain remnant patches of soil-hosted ground ice formed during the last ground-ice maximum, whereas the poleward limit marks where the ice-cemented mantle persists and is stable.

The MOC images and their distribution indicate the following sequence of events for the formation and evolution of this terrain. (1) Under favourable orbital configurations, airfall dust is permeated and cemented by atmospherically deposited ice through a diffusion and condensation process. (2) Changes in insolation driven by the precession of the equinoxes and variations in obliquity lead to surface and soil conditions where ice is no longer stable. (3) Destabilization of the surface (pits, cracks, or sags due to cyrospheric processes) allow devolatilization of the near-surface ground ice. (4) The devolatilized dust is analogous to desiccated loess and can be disaggregated and removed by atmospheric processes. (5) Removal of the ice-cemented soil layer reveals the pre-existing surface. With continued orbital variations, this process can repeat itself numerous times over timescales of 10^6 years.

A layer of soil 1–10 m thick with the capacity to store and release water ice on timescales of 10^5 years has important implications for the transport and storage of water on Mars. The 30°–60° latitude bands are zones of active accumulation and release of ground ice. To estimate the fluxes of water due to this process we use a conservative estimate of 3 m for the active ground ice layer with a porosity range of 10–40%. This results in 30–110 g cm^{-2} of water cycled within these latitude bands, which, integrated over the latitude bands, is equivalent to a global layer of water between 10 cm and 40 cm thick or a total volume of $(1.5–6.0) \times 10^4$ km^3. These observations provide direct evidence for a ground ice cycle on Mars operating on Milankovich timescales. This ground ice cycle is the modern manifestation of martian ice ages and has significantly modified the martian surface. □

Received 22 December 2000; accepted 5 June 2001.

1. Squyres, S. W. Urey Prize Lecture: Water on Mars. *Icarus* **79,** 229–288 (1989).
2. Carr, M. H. *Water on Mars* (Oxford Univ. Press, New York, 1996).
3. Clifford, S. M. A model for the hydrologic and climatic behavior of water on Mars. *J. Geophys. Res.* **98,** 10973–11016 (1993).
4. Fanale, F. P., Salvail, J. R., Zent, A. P. & Postawko, S. E. Global distribution and migration of subsurface ice on Mars. *Icarus* **67,** 1–18 (1986).
5. Squryes, S. W. & Carr, M. H. Geomorphic evidence for the distribution of ground ice on Mars. *Science* **231,** 249–252 (1986).
6. Houben, W., Haberle, R. M., Young, R. E. & Zent, A. P. Modeling the martian seasonal water cycle. *J. Geophys. Res.* **102,** 9069–9094 (1997).
7. Mellon, M. T. & Jakosky, B. M. The distribution and behavior of Martian ground ice during past and present epochs. *J. Geophys. Res.* **100,** 11781–11799 (1995).
8. Malin, M. C. *et al.* Early view of Martian surface from the mars Orbiter Camera of Mars Global Surveyor. *Science* **279,** 1681–1685 (1998).
9. Edgett, K. S. & Malin, M. C. New views of Mars eolian activity, materials, and surface properties: Three vignettes from the Mars Global Surveyor Mars Orbiter Camera. *J. Geophys. Res.* **105,** 1623–1650 (2000).
10. Christensen, P. R. & Moore, H. J. in *Mars* (eds Kieffer, H. H., Jakosky, B. M., Snyder, C. W. & Matthews, M. S.) 686–729 (Univ. Arizona Press, Tuscon, 1992).
11. Cooper, C. D. & Mustard, J. F. Criteria for remote sensing detection of sulfate cemented soils on Mars. *Lunar Planet. Sci.* [online] **31,** 1747 (2000).
12. Mustard, J. F. Recent ground ice on Mars and implications for volatiles and surface processes. *Lunar Planet. Sci.* [online] **32,** 1988 (2001).

13. Seibert, N. M. & Kargel, J. S. Small-scale martian polygonal terrain: Implications for liquid surface water. *Geophys. Res. Lett.* **28,** 899–902 (2001).
14. Johnson, J. J. & Lorenz, R. D. Thermophysical properties of Alaskan loess: An analog material for the martian polar layered terrain? *Geophys. Res. Lett.* **27,** 2769–2772 (2000).
15. Storrs, A. D., Fanale, F. P., Saunders, R. S. & Stephens, J. B. The formation of filamentary sublimate residues (FSR) from mineral grains. *Icarus* **76,** 493–512 (1988).
16. Haberle, R. M., Houben, W., Barnes, J. R. & Young, R. E. A simplified three-dimensional model for Martian climate studies. *J. Geophys. Res.* **102,** 9051–9068 (1997).
17. Metzger, S. M. *et al.* Dust devil vortices seen by the Mars Pathfinder camera. *Geophys. Res. Lett.* **26,** 2781–2784 (1999).
18. Renno, N. O. *et al.* Martian and terrestrial dust devils: Test of a scaling theory using Pathfinder data. *J. Geophys. Res.* **105,** 1859–1865 (2000).
19. Herkenhoff, K. E. & Plaut, J. J. Surface ages and resurfacing rates of the polar layered deposits on Mars. *Icarus* **144,** 243–253 (2000).
20. Kreslavsky, M. A. & Head, J. W. Kilometer scale roughness of Mars: Results from MOLA data analysis. *J. Geophys. Res.* **105,** 26695–26712 (2000).

Acknowledgements

Discussions were provided by J. Head and P. Schultz and formal reviews were provided by M. Carr and B. Jakosky. The efforts of the MOC science team in creating the data base is gratefully acknowledged. This work is supported by grants from NASA.

Correspondence and requests for materials should be addressed to J.F.M. (e-mail: john_mustard@brown.edu).

In situ detection of collisionless reconnection in the Earth's magnetotail

M. Øieroset*, T. D. Phan*, M. Fujimoto†, R. P. Lin* & R. P. Lepping‡

* *Space Sciences Laboratory, University of California, Berkeley, California 94720, USA*
† *Department of Earth and Planetary Sciences, Tokyo Institute of Technology, Meguro 152, Japan*
‡ *NASA Goddard Space Flight Center, Code 696, Greenbelt, Maryland 20771, USA*

Magnetic reconnection is the process by which magnetic field lines of opposite polarity reconfigure to a lower-energy state, with the release of magnetic energy to the surroundings. Reconnection at the Earth's dayside magnetopause and in the magnetotail allows the solar wind into the magnetosphere[1,2]. It begins in a small 'diffusion region', where a kink in the newly reconnected lines produces jets of plasma away from the region. Although plasma jets from reconnection have previously been reported[3–7], the physical processes that underlie jet formation have remained poorly understood because of the scarcity of *in situ* observations of the minuscule diffusion region. Theoretically, both resistive and collisionless processes can initiate reconnection[8–14], but which process dominates in the magnetosphere is still debated. Here we report the serendipitous encounter of the Wind spacecraft with an active reconnection diffusion region, in which are detected key processes predicted by models[8–13] of collisionless reconnection. The data therefore demonstrate that collisionless reconnection occurs in the magnetotail.

When magnetic field lines of opposite polarity convect toward each other they reconnect and change configuration in a small diffusion region centred around a magnetic X-line (Fig. 1). Outside the diffusion region, in the inflow as well as the high-speed jet regions, the magnetic field lines are 'frozen' to the plasma. In the diffusion region, however, the field lines diffuse from the plasma, allowing the opposite field lines to merge and change partners (Fig. 1b). The occurrence of reconnection depends critically on the plasma processes within the diffusion region. Essentially all of the experimental tests for its occurrence, however, pertain to observations outside the diffusion region. Much of our knowledge of processes in the diffusion region thus derives solely from theoretical modelling[8–15].

According to theory, reconnection can be accomplished either by resistive or by collisionless mechanisms. The classical collision rate in the magnetosphere is low, but anomalous resistivity could be provided by increased wave activity[15–17]. If the resistive scale size is larger than the ion scale size (the ion skin depth—see Fig. 1 for definition), reconnection is accomplished by resistive diffusion of ions and electrons at the resistive scale and no separation between ions and electrons occurs. If, on the other hand, the resistive scale size is smaller than the ion skin depth, collisionless effects become dominant, and a separation of ions and electrons (the Hall effect) occurs as the ions are first unfrozen from the magnetic field (at the larger ion scale) while the electrons continue to carry the field lines toward the X-line and eventually diffuse at the smaller electron scale[14]. The separation between electrons and ions in the ion diffusion region gives rise to a system of currents, termed the 'Hall current' (see Fig. 1b), which in turn induces a quadrupolar out-of-plane Hall magnetic field pattern[8]. The Hall quadrupolar fields should be recognizable by a spacecraft traversing the magnetotail reconnection region, from one side of the X-line to the other, as a reversal of the out-of-plane component (y-component) of the magnetic field, with an amplitude of ~30% of the background magnetospheric field[18]. Electrons carrying the Hall current are expected along the boundary separating the lobe and the plasma sheet[19–21].

Out-of-plane magnetic fields have recently been detected by the Geotail spacecraft in the high-speed flow region outside the diffusion region both in the near-Earth tail[21] and at the dayside magnetopause[22]. These fields are presumably the extensions of the Hall magnetic fields originating inside the diffusion region. But as long as such signatures are obtained only outside the diffusion region one cannot tell with certainty whether the observed signatures are the cause or consequence of reconnection. Only *in situ* detection of Hall signatures in the diffusion region would unambiguously point to the dominance of collisionless effects in magnetic reconnection.

The Wind spacecraft made a fortuitous direct encounter with the ion diffusion region on 1 April 1999. As the spacecraft travelled away from the Sun through the Earth's magnetotail (see Fig. 1), at about 60 Earth radii behind the Earth it detected a period of Earthward-directed plasma jets followed by an interval of tailward-directed jets, with proton flow speed reaching 400 km s^{-1} (Fig. 2b). The velocities of both the Earthward and tailward jets are in agreement with the predicted slingshot effect resulting from reconnection[7]. This flow interval was embedded in a 10-hour interval of quasi-steady reconnection[7]. The detection of the reversal of the reconnection jets implies that the spacecraft moved from the Earthward side to the tailward side of an active reconnection X-line (Fig. 1b). The spacecraft remained in the reconnection layer as it crossed from one side of the X-line to the other, as evident from the uninterrupted transition from Earthward to tailward flow (Fig. 2a), so the spacecraft must have crossed the diffusion region. If the crossing from one side of the X-line to the other had occurred outside the diffusion region, the spacecraft would have detected an interval of slow flow in the z-direction only, which corresponds to the reconnection inflow region[7]. It can be inferred from the mostly negative sign of the x-component of the magnetic field, B_x, that the spacecraft stayed predominantly on the southward side of the plasma sheet midplane (the neutral sheet) during the crossing near the X-line, as schematically shown in Fig. 1b.

We now describe the Hall electron and magnetic field signatures obtained in the diffusion region implying that collisionless (rather than resistive) effects dominate in this event.

As the spacecraft travelled from the region of Earthward jets to the region of tailward jets while remaining mostly below the plasma